Vibrational Excitation Mechanism in Tunneling Spectroscopy beyond the Franck-Condon Model

Gaël Reecht,[1] Nils Krane,[1] Christian Lotze,[1] Lei Zhang,[2] Alejandro L. Briseno,[2] and Katharina J. Franke[1]
[1]Fachbereich Physik, Freie Universität Berlin, Arnimallee 14, 14195 Berlin, Germany
[2]Department of Polymer Science and Engineering, University of Massachusetts, Amherst, Massachusetts 01003, USA

(Received 11 October 2019; revised manuscript received 22 January 2020; accepted 21 February 2020; published 20 March 2020)

Vibronic spectra of molecules are typically described within the Franck-Condon model. Here, we show that highly resolved vibronic spectra of large organic molecules on a single layer of MoS_2 on Au(111) show spatial variations in their intensities, which cannot be captured within this picture. We explain that vibrationally mediated perturbations of the molecular wave functions need to be included into the Franck-Condon model. Our simple model calculations reproduce the experimental spectra at arbitrary position of the scanning tunneling microscope's tip over the molecule in great detail.

DOI: 10.1103/PhysRevLett.124.116804

Vibronic excitations are resonant transitions from a molecular ground state to an electronically and vibrationally excited state. These excitations are typically described by the Franck-Condon model. The essence of it are fast electronic transitions treated in Born-Oppenheimer approximation, such that the excitations occur without changes in the nuclear coordinates or momentum. Vibronic excitations in single molecules on surfaces can be detected as resonant sidebands of positive or negative ion resonances in tunneling spectroscopy [1–7] with apparent submolecular variations due to distinct close-lying orbitals [8–10]. In contrast to these resonant excitations, inelastic vibrational excitations far below resonance [11–13] are described by a change in the nuclear coordinates, which leads to a modified tunneling matrix element and to the opening of a new tunneling path [14–16]. Hence, off-resonant inelastic tunneling and resonant vibronic transitions are treated in distinct and complementary models [17]. The combination of both models would be akin to phonon-mediated electronic transitions in crystal structures [18,19], where the activation of a phonon mode enables otherwise forbidden electronic transitions, as the initial and final state have different parallel momentum in the electronic band structure [20–23]. Signatures of such combined excitations in single molecules have not been reported to date.

Recent tunneling experiments have revealed some limitations of the Franck-Condon model. In cases where the electronic energy level spacing was similar to vibrational energies, it was found that avoided level crossings determine the resonant sidebands [24,25]. In other cases, intensity variations of the resonant sidebands along an organic molecule were interpreted in terms of coherent vibrational modes with different symmetries [8] or with vibration-assisted coupling of wave functions of different symmetry in molecule and tip [26]. Selection rules could not be derived, because the vibrational modes and associated nuclear displacements of the molecule could not be identified owing to an insufficient experimental energy resolution probably limited by nonadiabatic relaxation effects.

Here, we show that vibration-assisted tunneling and Franck-Condon excitations are crucial for a complete vibronic model. To benchmark our model we use vibronic spectra of large organic molecules on a single layer of MoS_2 on Au(111). The van der Waals layer acts as an efficient decoupling layer from the metal substrate and provides exceptional energy resolution of a few millielectronvolts [27–29]. This allows us to probe vibronic states and their modulation of intensities with intramolecular resolution. We show that the spatial intensity variations can be simulated by adding vibration-assisted tunneling to the Franck-Condon picture.

Scanning tunneling microscopy (STM) experiments were performed at a temperature of 4.6 K in ultrahigh vacuum. Monolayer islands of MoS_2 were grown on a clean Au(111) surface by depositing Mo in an H_2S atmosphere (5×10^{-5} mbar) and annealing to 800 K [30,31]. 2,5-Bis(3-dodecylthiophen-2-yl)thieno[3,2-b]thiophene (BTTT) [phthalocyanine (H_2Pc)] molecules were evaporated at 365 K [680 K] onto the surface held at 200 K [120 K]. Differential conductance (dI/dV) spectra and maps were recorded using lock-in detection with 921 Hz modulation frequency.

The deposition of BTTT molecules on MoS_2 leads to partially ordered structures with the molecules lying parallel to each other [Fig. 1(a)] [37]. dI/dV spectra recorded at the extremity of a BTTT (red curve) and on the bare MoS_2 (gray curve) are presented in Fig. 1(b). The spectrum on MoS_2 shows the well characterized semiconducting band gap (~ -1.4 V to $+0.5$ V) [38], which is essential for decoupling the molecules from the substrate [27,29]. The spectrum on the BTTT molecule shows a

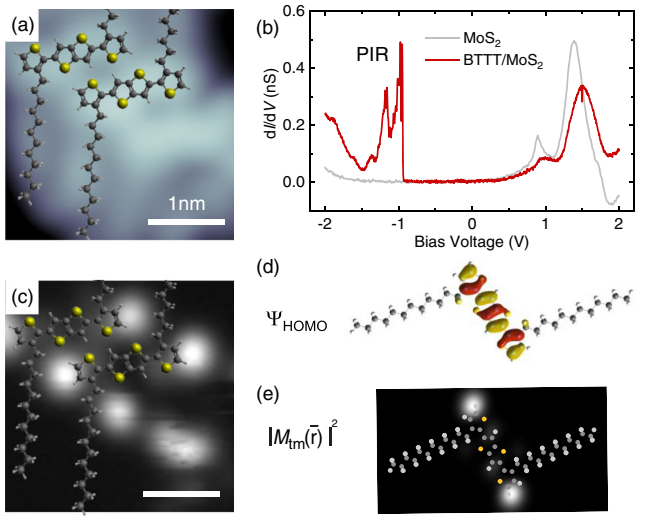

FIG. 1. (a) STM topography of BTTT on $MoS_2/Au(111)$ with overlaid molecular model ($I = 20$ pA, $V = 1$ V). (b) dI/dV spectra recorded over bare MoS_2 (gray) and BTTT (red) (feedback opened at 150 pA, 2.2 V; $V_{mod} = 10$ mV). (c) Constant-height dI/dV map of the same area as (a) at $V = -0.975$ V ($V_{mod} = 10$ mV). (d) DFT-calculated HOMO isodensity (Ψ_{HOMO}) of BTTT, and (e) position-dependent calculation of the tunneling matrix element $|M_{tm}(\vec{r})|^2$ between Ψ_{HOMO} and an s-type wave function Ψ_t of the STM tip (tip-molecule distance 8.5 Å [32,33]).

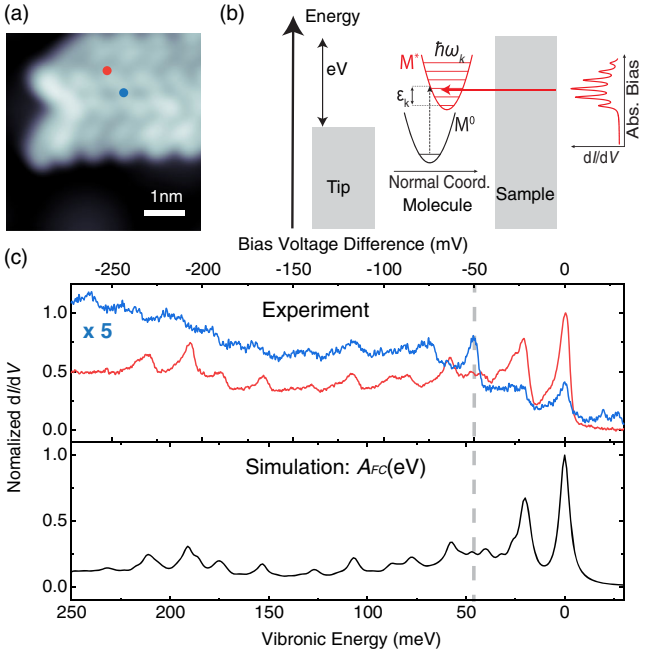

FIG. 2. (a) STM topography of BTTT on $MoS_2/Au(111)$ ($I = 10$ pA, $V = 0.9$ V). (b) Sketch of vibrational excitation mechanism of a molecule in an STM junction. (c) Top: dI/dV spectra at the PIR of BTTT recorded at the same tip height on two different positions of the same molecule [see corresponding dots in (a)]. Spectra are normalized to the largest intensity of the red spectrum. The blue spectrum is then enlarged by a factor of 5 and shifted in energy to the same elastic peak (feedback opened at 250 pA, −1.2 V at extremity, $V_{mod} = 0.5$ mV). Bottom: simulated dI/dV vibronic spectrum considering the Franck-Condon mechanism described in (b), energy broadening set to FWHM = 6 mV. The upper and lower axis differ by 10% to account for the voltage drop in MoS_2.

positive ion resonance (PIR) inside this gap at ~ -1 V. This resonance exhibits a rich satellite structure revealing the vibronic properties of the molecule. The intensity of this resonance is largest at the ends of the thiophene backbone [dI/dV map in Fig. 1(c)]. At first sight this shape does not agree with the delocalized nature of the highest occupied molecular orbital (HOMO) [Fig. 1(d)]. However, we note that the conductance signal in STM is proportional to the square of the tunneling matrix element M_{tm}, which depends on the overlap of the wave functions Ψ_t of the tip and Ψ_m of the molecule [39].

We simulate the position-dependent tunneling matrix element along the BTTT molecule by assuming an s-type wave function for the STM tip and the molecular wave function derived from density functional theory (DFT) (details in Supplemental Material [33]). The simulation for the HOMO [Fig. 1(e)] is in good agreement with the constant-height dI/dV map of the positive ion resonance inside the gap [Fig. 1(c)].

We now focus on the study of the vibrational properties of BTTT. Highly resolved spectra of the satellite structure of the PIR recorded at the extremity (red) and in the center (blue) of the thiophene backbone are shown in Fig. 2(c). Both spectra are normalized to the highest-intensity peak of the red spectrum, and a factor of 5 is additionally applied to the blue one for clarity. Furthermore, they are shifted to the same onset energy, i.e., to the elastic peak, to eliminate the effect of the inhomogeneous tip potential over the molecule [28] (see raw data in Supplemental Material [33]). We first discuss the spectrum recorded at the extremity of the molecule, corresponding to the position of the highest tunneling probability into the HOMO-derived resonance [see Fig. 1(c)]. As described in a previous work on BTTT, the vibronic fingerprint at this site can be explained within the Franck-Condon picture [27]. The excitation probability of a vibrational mode k and its harmonics is given by the overlap integral of the initial (ground state) and final state. It depends on the relaxation energy ϵ_k when charging the molecule, as sketched in Fig. 2(b). The relaxation energy of each vibrational mode can be derived from gas-phase DFT calculations of the neutral and the positively charged molecular state (details in Supplemental Material [33]). A simulated Franck-Condon spectrum $A_{FC}(eV)$ for the BTTT molecule is shown in the bottom panel of Fig. 2(c). It is in remarkable agreement with the experimental spectrum recorded at the extremity of the molecule (red). Note that a scaling factor is required between the calculated vibronic energy (bottom axis) and the bias voltage of experimental dI/dV spectra (top axis), accounting for the voltage drop in the MoS_2 layer (~10%).

Considering only the Franck-Condon principle, the relative intensities of the vibronic resonances should be constant along the molecule. This is in contrast to the experimentally observed spatial variations of excitation efficiencies along the molecule in Fig. 2(c). The spectrum at the center of the BTTT molecule exhibits different intensity ratios of the vibronic peaks from the spectrum at the extremities. Most striking is a strongly enhanced peak at ~50 meV above the elastic peak (dashed line) [40]. We will show that this additional peak can be explained by an additional excitation mechanism.

Pavlicek *et al.* [26] have recently explained spatial variations of vibronic excitations by the coupling of wave functions of different symmetry in the tip and molecule. However, the vibronic peaks were of several tens of millielectronvolts width probably due to nonadiabatic coupling to substrate phonons in the ionic NaCl substrate [41]. The lack of energy resolution thus prevented the identification of the involved vibrational modes. Consequently, the determination of selection rules of this excitation was not possible. To explain the spatial variation of the vibronic signature across the BTTT molecule, we propose the following mechanism. In addition to the Franck-Condon picture [process 1 in Fig. 3(b)] we also consider vibration-assisted tunneling [VAT; process 2 in Fig. 3(b)] The latter is in analogy to the off-resonant inelastic excitation, also referred to as inelastic electron tunneling spectroscopy. As discussed before, the tunneling probability into a molecular orbital (MO) is determined by the overlap of the tip and MO electronic wave function. This overlap is strongly reduced for an *s*-wave tip at the center of the BTTT, due to the symmetry of the HOMO's nodal planes [see Figs. 1(c) and 1(e) and scheme in Fig. 3(a)]. In VAT, this symmetry can be broken by a vibrational mode of the molecule as shown in Fig. 3(a). Here, an out-of-plane mode with an antisymmetric character relative to the HOMO's nodal planes leads to an increasing (decreasing) overlap between the tip and the parts of the molecular wave function with a positive (negative) sign, or vice versa. Such a change of the wave function allows for a large (vibration-assisted) tunneling matrix element [14,25] and effectively opens a new tunneling channel at the threshold of the vibrational excitation, i.e., at $E_V = E_H + \hbar\omega_k$, with E_H being the elastic excitation of the HOMO [see scheme in Figs. 3(a) and 3(b)]. In contrast to off-resonant inelastic tunneling, resonant VAT includes an electronic excitation according to the Franck-Condon principle and an additional inelastic transition within the excited state. This combination leads to a replicas of the Franck-Condon spectrum at higher energies [Fig. 3(b)].

To analyze which vibrations give rise to a large VAT matrix element, we assume—in analogy to off-resonant inelastic excitation—the tunneling probability of the newly opened channel to depend on the overlap between the

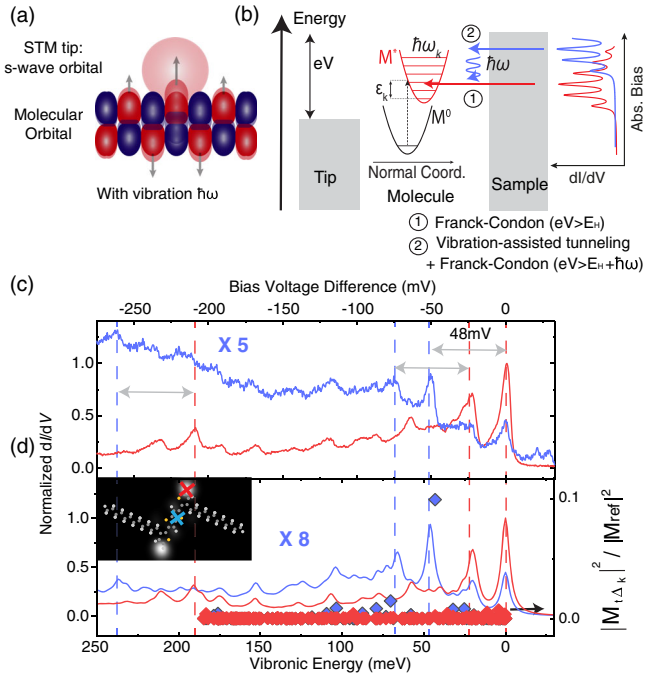

FIG. 3. (a) Schematic representation of vibration-assisted tunneling: when the tip is placed over the center of the molecule, the overlap between the tip and molecule wave function is small due to the nodal planes. Considering a vibrational distortion of the molecule the overlap can be modified. If the overlap is increased, the tunneling matrix element is increased and a new inelastic channel is opened, as sketched in (b). (c) Experimental spectra of Fig. 2(c) of the PIR at two different tip positions (center: blue; extremity: red). (d) Diamonds (right axis): calculated change of the tunneling matrix element $|M_{t\Delta_k}(\vec{r})|^2$ for all vibrational modes k of BTTT, for a tip position similar to the experimental spectra in (b) (see map and model with crosses in inset, tip height 8.5 Å). $|M_{t\Delta_k}(\vec{r})|^2$ are given in units of M_{ref} being the maximum value of M_{tm}, i.e., at the extremity of the molecule. Line (left axis): simulated spectra for the same tip positions including vibration-assisted tunneling using Eq. (2).

s-wave tip and perturbed molecular wave function $\delta Q_k(\partial\Psi_m/\partial Q_k)$ [14,16]. In our calculation we approximate it by

$$\delta Q_k \frac{\partial \Psi_m}{\partial Q_k} \approx \delta Q_k \frac{\Delta \Psi_m}{\Delta Q_k} = \frac{\Psi_{m,k+} - \Psi_{m,k-}}{2} = \frac{\Delta \Psi_{m,k}}{2}, \qquad (1)$$

with $\Psi_{m,k\pm}$ being the wave function for the vibrationally excited molecule, displaced by $\pm\delta Q_k$ as determined from DFT calculations of the free molecule (details in Supplemental Material [33]). Thus, we calculate the VAT matrix element $|M_{t\Delta_k}(\vec{r})|^2$ (see Eq. S6 in Supplemental Material [33]) for the perturbed molecular wave function at the center and extremity of the BTTT molecule for each mode [Fig. 3(d) (diamonds)]. At the center of the molecule, one vibrational mode at 43.1 meV yields a large change of the tunneling matrix element. Considering the voltage drop in the MoS_2 layer (~10%), this is in good agreement with

the additional peak at ~50 meV in the experimental dI/dV spectrum (blue spectrum). This mode corresponds to an out-of-plane mode, mainly localized on the thienothiophene unit (see Supplemental Material [33]). In contrast, at the molecular extremity the change in tunneling matrix element is negligible for all modes. Thus, spectra taken at this position can be explained by considering only the Franck-Condon principle.

In order to merge the two excitation mechanisms, we consider that the VAT adds another tunneling channel to the excited molecule (in its PIR) of intensity $|M_{t\Delta_k}(\vec{r})|^2$, which then has to be convolved with the Franck-Condon spectrum $A_{\mathrm{FC}}(eV)$. As a result, the Franck-Condon peaks are replicated at energies shifted by $\hbar\omega_k$. A fingerprint of this can be seen by the repetition of the pattern of the most intense peaks indicated by red and blue dashed lines in Fig. 3(c). Thus, the position-dependent vibronic intensities can be calculated as (details in Supplemental Material [33]):

$$A_{\mathrm{total}}(\vec{r}, eV) = |M_{\mathrm{tm}}(\vec{r})|^2 \cdot A_{\mathrm{FC}}(eV) + \sum_k |M_{t\Delta_k}(\vec{r})|^2 \cdot A_{\mathrm{FC}}(eV + \hbar\omega_k). \quad (2)$$

Note that the only free parameter for the simulation is the tip-molecule distance (discussion in Supplemental Material [33]). Figure 3(d) shows the simulated spectra for the tip over the center (blue) and extremity (red) of the molecule for a tip-molecule distance of 8.5 Å [32]. Both are now in good agreement with the experimental spectra. Equivalent simulations can be carried out at an arbitrary position over the molecule [33].

To validate our full vibronic model, we now turn to a second molecular system: phthalocyanine (H_2Pc). This molecule appears with a clover shape when scanned at low bias voltages [Fig. 4(a)] and exhibits—as BTTT—a sharp PIR in the semiconducting MoS_2 gap [29] (see large-scale spectra in Supplemental Material [33]), associated with the removal of one electron from its HOMO. The dI/dV map recorded at the energy of the PIR shows eight lobes, two lobes next to each isoindole moiety [Fig. 4(d)(i)]. As for BTTT, this map can be simulated [Fig. 4(e)(i)] by considering the tunneling matrix element between an s-wave tip and the DFT-calculated HOMO wave function of H_2Pc [Fig. 4(b)]. Highly resolved spectra of the PIR recorded over one of this eight lobes show mainly one sharp elastic peak [black spectrum in Fig. 4(c)]. At this position, there is hardly any intensity in the vibronic sidebands. This can be understood by a small relaxation energy $\epsilon_{\mathrm{rel}} = 21.7$ meV of H_2Pc upon positive charging (simulated Franck-Condon spectrum in Supplemental Material [33]).

In contrast, spectra over the isoindoline moieties show a pronounced set of peaks above the elastic peak [Fig. 4(c)]. The peaks can be classified into three groups (α, β, and γ) according to their spatial distribution in the respective dI/dV maps [see experimental maps in Figs. 4(d)(ii)–4(d)(iv)]. While all maps show the eight-lobe structure (with varying intensity), the α resonances show additional intensity on the macrocycle, the γ's have very strong weight on the center and β's show some conductance on the macrocycle and the center (all maps in Supplemental Material [33]).

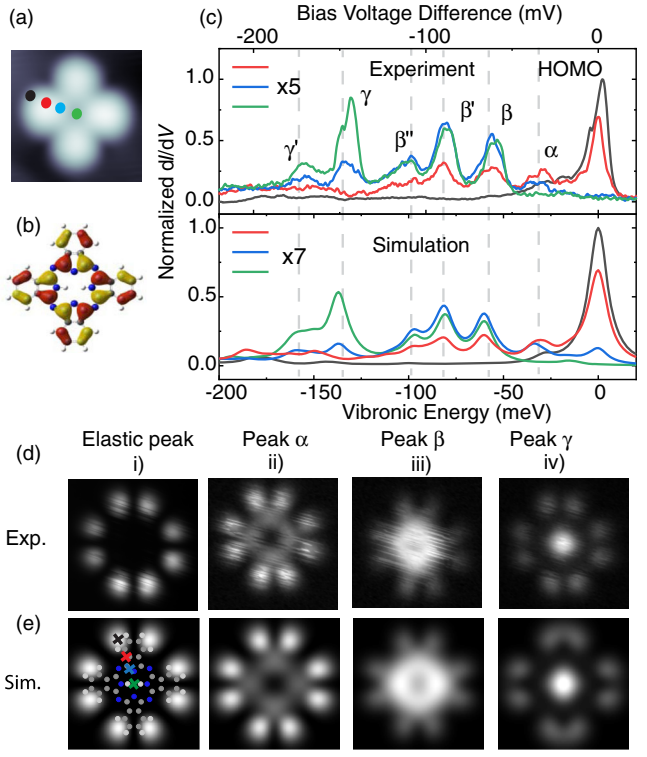

FIG. 4. (a) 2.4×2.4 nm^2 STM topography of H_2Pc on MoS_2/Au(111) ($I = 20$ pA, $V = 0.5$ V). (b) DFT-calculated HOMO isodensity of H_2Pc. (c) Top: dI/dV spectra recorded at the same tip height at positions shown by dots in (a) (feedback opened at 40 pA, −1.2 V on lobe of H_2Pc, $V_{\mathrm{mod}} = 2$ mV). Spectra are normalized to the elastic peak of the black spectrum. Additionally, the red, blue, and green spectra are scaled by a factor of 5 for clarity. All spectra are shifted to the same energy of the elastic peak. Bottom: simulated spectra for tip positions indicated as crosses in (e), tip height 7.5 Å. (d) 2.4×2.4 nm^2 constant-height dI/dV maps at energies corresponding to (i) the elastic peak (HOMO) and (ii)–(iv) α, β, and γ inelastic peaks in (b) ($V_{\mathrm{mod}} = 5$ mV). (e) Corresponding simulated conductance maps.

To show that these position-dependent resonances result from the above derived picture of a combination of VAT and Franck-Condon excitations, we calculate the VAT matrix element of the vibrationally perturbed molecular wave functions with an s-wave tip. We find a large number of vibrational modes, which cause an increase of the VAT matrix element [33]. The corresponding calculated dI/dV spectra [according to Eq. (2), bottom panel of Fig. 4(c)] are in excellent agreement with the experimental spectra. We note that the elastic peak can be of much lower intensity than the inelastic satellites. To prove that our model

reproduces the spatial distribution of the VAT, we also simulate the conductance maps at the energies of the different vibrational modes involved in the transport, which are in remarkably good agreement with the experimental maps [Fig. 4(e)].

In conclusion, our highly resolved tunneling spectra of molecules on a monolayer of MoS_2 revealed evidence of the interplay of two distinct excitation mechanisms of molecular vibrations. On the one hand, tunneling electrons resonantly excite vibrational modes which can be described within the Franck-Condon model. On the other hand, inelastic tunneling electrons excite molecular vibrations, which facilitate tunneling into the molecule at positions, where it would be suppressed in the static case for symmetry reasons. We could describe all spectral details of vibrational intensities by combining vibration-assisted tunneling (VAT) and the Franck-Condon principle. We note that VAT may enhance higher-energy resonances over the elastic onset. In the case of less resolved spectra, this may cause an apparent shift of peaks. Furthermore, our description of VAT is not restricted to STM experiments, it may also affect charge transport through organic materials and heteromolecular interfaces.

This work was supported by the Deutsche Forschungsgemeinschaft (DFG)—Project No. 182087777—SFB 951, and by the European Research Council (ERC) through the Consolidator Grant "NanoSpin." We gratefully acknowledge discussions with M.-L. Bocquet and A. Donarini.

[1] X. H. Qiu, G. V. Nazin, and W. Ho, Phys. Rev. Lett. **92**, 206102 (2004).
[2] N. A. Pradhan, N. Liu, and W. Ho, J. Phys. Chem. B **109**, 8513 (2005).
[3] G. V. Nazin, S. W. Wu, and W. Ho, Proc. Natl. Acad. Sci. U.S.A. **102**, 8832 (2005).
[4] T. Frederiksen, K. J. Franke, A. Arnau, G. Schulze, J. I. Pascual, and N. Lorente, Phys. Rev. B **78**, 233401 (2008).
[5] F. Matino, G. Schull, F. Köhler, S. Gabutti, M. Mayor, and R. Berndt, Proc. Natl. Acad. Sci. U.S.A. **108**, 961 (2011).
[6] F. Schulz, R. Drost, S. K. Hämäläinen, and P. Liljeroth, ACS Nano **7**, 11121 (2013).
[7] S. Wickenburg, J. Lu, J. Lischner, H.-Z. Tsai, A. A. Omrani, A. Riss, C. Karrasch, A. Bradley, H. S. Jung, R. Khajeh, D. Wong, K. Watanabe, T. Taniguchi, A. Zettl, A. H. C. Neto, S. G. Louie, and M. F. Crommie, Nat. Commun. **7**, 13553 (2016).
[8] N. Ogawa, G. Mikaelian, and W. Ho, Phys. Rev. Lett. **98**, 166103 (2007).
[9] Q. Huan, Y. Jiang, Y. Y. Zhang, U. Ham, and W. Ho, J. Chem. Phys. **135**, 014705 (2011).
[10] A. Mehler, N. Néel, M.-L. Bocquet, and J. Kröger, J. Phys. Condens. Matter **31**, 065001 (2019).
[11] B. C. Stipe, M. A. Rezaei, and W. Ho, Science **280**, 1732 (1998).
[12] A. J. Heinrich, C. P. Lutz, J. A. Gupta, and D. M. Eigler, Science **298**, 1381 (2002).
[13] W. Ho, J. Chem. Phys. **117**, 11033 (2002).
[14] N. Lorente and M. Persson, Phys. Rev. Lett. **85**, 2997 (2000).
[15] N. Lorente, Appl. Phys. A **78**, 799 (2004).
[16] S. Burema, N. Lorente, and M.-L. Bocquet, J. Chem. Phys. **136**, 244507 (2012).
[17] K. J. Franke and J. I. Pascual, J. Phys. Condens. Matter **24**, 394002 (2012).
[18] A. G. Chynoweth, R. A. Logan, and D. E. Thomas, Phys. Rev. **125**, 877 (1962).
[19] L. Eaves, P. S. S. Guimares, B. R. Snell, D. C. Taylor, and K. E. Singer, Phys. Rev. Lett. **55**, 262 (1985).
[20] Y. Zhang, V. W. Brar, F. Wang, C. Girit, Y. Yayon, M. Panlasigui, A. Zettl, and M. F. Crommie, Nat. Phys. **4**, 627 (2008).
[21] T. O. Wehling, I. Grigorenko, A. I. Lichtenstein, and A. V. Balatsky, Phys. Rev. Lett. **101**, 216803 (2008).
[22] F. D. Natterer, Y. Zhao, J. Wyrick, Y.-H. Chan, W.-Y. Ruan, M.-Y. Chou, K. Watanabe, T. Taniguchi, N. B. Zhitenev, and J. A. Stroscio, Phys. Rev. Lett. **114**, 245502 (2015).
[23] E. E. Vdovin, A. Mishchenko, M. T. Greenaway, M. J. Zhu, D. Ghazaryan, A. Misra, Y. Cao, S. V. Morozov, O. Makarovsky, T. M. Fromhold, A. Patanè, G. J. Slotman, M. I. Katsnelson, A. K. Geim, K. S. Novoselov, and L. Eaves, Phys. Rev. Lett. **116**, 186603 (2016).
[24] J. Repp, P. Liljeroth, and G. Meyer, Nat. Phys. **6**, 975 (2010).
[25] F. Schwarz, Y. F. Wang, W. A. Hofer, R. Berndt, E. Runge, and J. Kröger, J. Phys. Chem. C **119**, 15716 (2015).
[26] N. Pavlicek, I. Swart, J. Niedenführ, G. Meyer, and J. Repp, Phys. Rev. Lett. **110**, 136101 (2013).
[27] N. Krane, C. Lotze, G. Reecht, L. Zhang, A. L. Briseno, and K. J. Franke, ACS Nano **12**, 11698 (2018).
[28] N. Krane, C. Lotze, N. Bogdanoff, G. Reecht, L. Zhang, A. L. Briseno, and K. J. Franke, Phys. Rev. B **100**, 035410 (2019).
[29] G. Reecht, N. Krane, C. Lotze, and K. J. Franke, ACS Nano **13**, 7031 (2019).
[30] S. S. Grønborg, S. Ulstrup, M. Bianchi, M. Dendzik, C. E. Sanders, J. V. Lauritsen, P. Hofmann, and J. A. Miwa, Langmuir **31**, 9700 (2015).
[31] N. Krane, C. Lotze, J. M. Läger, G. Reecht, and K. J. Franke, Nano Lett. **16**, 5163 (2016).
[32] For the calculation of the tunneling matrix element, the tip-molecule distance is defined between the center of the *s*-type wave function and the center of the molecule. This value is therefore larger than the distance of the tip to contact formation with the molecule.
[33] See Supplemental Material at http://link.aps.org/supplemental/10.1103/PhysRevLett.124.116804 for (i) simulation details, (ii) additional data on BTTT and H_2Pc, (iii) detailed analysis of involved vibrational modes, (iv) height dependence of VAT model, (v) more details of the calculation of the tunneling matrix element, which includes Refs. [34–36].
[34] M. J. Frisch, G. W. Trucks, H. B. Schlegel, G. E. Scuseria, M. A. Robb, J. R. Cheeseman, G. Scalmani, V. Barone, G. A. Petersson, H. Nakatsuji, X. Li, M. Caricato,

A. Marenich, J. Bloino, B. G. Janesko, R. Gomperts, B. Mennucci, H. P. Hratchian, J. V. Ortiz, A. F. Izmaylov *et al.*, *Gaussian 09, Revision d.01* (Gaussian Inc., Wallingford, CT, 2009).

[35] J. Tersoff and D. R. Hamann, Phys. Rev. B **31**, 805 (1985).

[36] E. B. Wilson, J. C. Decius, and P. C. Cross, *Molecular Vibrations* (McGraw-Hill, London, 1955).

[37] The BTTT molecules can be found in two different adsorption configurations, which differ by rotation of the thiophene units with respect to the thienothiophene center around the C—C bonds. These configurations were classified as *trans-trans* and *cis-cis* rotamers. They exhibit a small shift of the positive ion resonance (PIR) and slight intensity and energy differences of the vibronic states [27]. In this Letter, we focus on the *trans-trans* rotamer.

[38] A. Bruix, J. A. Miwa, N. Hauptmann, D. Wegner, S. Ulstrup, S. S. Grønborg, C. E. Sanders, M. Dendzik, A. Grubisić Cabo, M. Bianchi, J. V. Lauritsen, A. A. Khajetoorians, B. Hammer, and P. Hofmann, Phys. Rev. B **93**, 165422 (2016).

[39] J. Bardeen, Phys. Rev. Lett. **6**, 57 (1961).

[40] If this peak was a second harmonic peak with higher intensity than the elastic peak, the Franck-Condon principle would predict an additional higher harmonic at ∼100 meV, which is not to be found.

[41] J. Repp, G. Meyer, S. Paavilainen, F. E. Olsson, and M. Persson, Phys. Rev. Lett. **95**, 225503 (2005).